

Study of the time-resolved, 3-dimensional current density distribution in solid metallic liners at 1 MA

S. C. Bott-Suzuki,^{1,a)} S. W. Cordaro,¹ L. S. Caballero Bendixsen,¹ L. Atoyan,² T. Byvank,² W. Potter,² B. R. Kusse,² J. B. Greenly,² and D. A. Hammer²

¹Center for Energy Research, University of California San Diego, La Jolla, California 92093, USA

²Laboratory for Plasma Studies, Cornell University, Ithaca, New York 14853, USA

(Received 26 July 2016; accepted 8 September 2016; published online 26 September 2016)

We present a study of the time varying current density distribution in solid metallic liner experiments at the 1 MA level. Measurements are taken using an array of magnetic field probes which provide 2D triangulation of the average centroid of the drive current in the load at 3 discrete axial positions. These data are correlated with gated optical self-emission imaging which directly images the breakdown and plasma formation region. Results show that the current density is azimuthally non-uniform and changes significantly throughout the 100 ns experimental timescale. Magnetic field probes show clearly motion of the current density around the liner azimuth over 10 ns timescales. If breakdown is initiated at one azimuthal location, the current density remains non-uniform even over large spatial extents throughout the current drive. The evolution timescales are suggestive of a resistive diffusion process or uneven current distributions among simultaneously formed but discrete plasma conduction paths. *Published by AIP Publishing.*

[<http://dx.doi.org/10.1063/1.4963249>]

INTRODUCTION

There has been considerable interest in the compression of cylindrical liner targets for hydrodynamics (e.g., Refs. 1 and 2) and inertial fusion studies (e.g., Refs. 3 and 4), most recently embodied by the MagLIF scheme under investigation at Sandia National Laboratories.⁵ The three-dimensional current density distribution in a metallic liner under compression by a fast-rising drive current is vital to the symmetry of the implosion in these systems. This determines the effective convergence ratio and hence achievable fuel compression in an ignition scenario. A z-pinch Inertial Fusion Energy (IFE) scheme will require rapid reloading of targets (e.g., Ref. 6), and accurate, repeatable electrical connection of the target to the electrode will be of great importance. Vacuum gaps in the power feed will breakdown on timescales determined by the applied voltage and gap parameters, typically leading to discrete locations where current can flow. In co-axial geometry, the locations and symmetry of such breakdowns will directly determine the profile of the downstream current distribution.

High voltage vacuum gaps are present in a variety of devices, including various switch designs and transmission line technologies. Breakdown asymmetries are important in determining the inductance of the system, but may also be reflected in the current flow. If such asymmetries occur far from a region of interest effects may be small if the current distribution becomes uniform after some distance. However, the azimuthal current distribution in coaxial geometries has received very little attention, and so the effects investigated here may be of importance in a range of related systems.

Recent studies by Blesener *et al.*⁷ and Awe *et al.*⁸ examined plasma formation where excellent current contacts around the azimuth at both electrodes were implemented for work using thin liners and shaped solid loads, respectively. In this work, we aim to investigate how the current density evolves from after being initially non-uniform, through use of a vacuum gap in the power feed, and if current distribution can become uniform over the axial length of a liner target at 1 MA. Since we cannot compress a fusion-scale liner design, we focus on the plasma initiation phase through both imaging and magnetic field measurements. We examine the spatial and temporal evolution of the current density throughout a liner using a magnetic field probe array. This method was first demonstrated in Cordaro *et al.*,⁹ and first applied to fusion-scale liners in Bott-Suzuki *et al.*¹⁰ In the latter study, we demonstrated that breakdown of a vacuum gap at the power feed can generate localized plasma regions and that this significantly affects the apparent current azimuthal uniformity at peak current. At UC San Diego, we recently extended these methodologies to 3-dimensions, using arrays of bdot probes at different axial locations along a conductor. Here, we apply this new approach to solid liners experiments on the 1 MA COBRA generator at Cornell University to examine the time evolution of the current distribution.

EXPERIMENTAL DESIGN

The load is driven by a voltage pulse applied to the AK (anode-cathode) gap at room temperature under a vacuum of $\sim 1 \times 10^{-5}$ Torr, and so breakdown is initiated by field emission processes. The liners are made from aluminum 1100 (pure aluminum) turned on a lathe with no further surface preparation. The liners are 3.05 mm in outer diameter, have a 150 μ m wall thickness, and are 30 mm in length. We ensure

^{a)}Electronic addresses: sbottsuzuki@ucsd.edu and p3ucsd.com

the liner makes good electrical contact with one end of the liner and establish a vacuum gap at the other, which is the subject of our analysis. All experiments presented here use a uniform 200 μm gap. Experiments were carried out on the COBRA machine at Cornell University.¹¹

The liner was fixed directly to the cathode using silver epoxy to ensure a good electrical contact. The anode plate was then placed over the liner, and an alignment cap was used to center the liner. The alignment cap is essentially a thin-walled tube, where the outer diameter is equal to the anode aperture, and the inner diameter is equal to the outer diameter of the liner. The cap therefore directly defines the vacuum gap. Both electrodes are fixed in place using the alignment cap, and finally, the cap is removed (Figure 1). This method allows excellent centering of the liner in the coaxial anode aperture.

The primary diagnostic method uses multiple magnetic field probes arranged around the liner each of which records the rate of change of the magnetic flux, dB/dt , throughout the experiment, with probe arrays at multiple axial positions (Figure 2). The probes are single loop probes formed from semi-rigid coaxial cables, with an approximate area of 0.1 mm^2 , insulated inside a $50 \mu\text{m}$ kapton tube and sealed with epoxy, similar to those in Ref. 12. Groups of bdot probes are shielded with an additional $50 \mu\text{m}$ kapton film, which maximizes re-use and limits the need to reposition and recalibrate probes between shots. Probes are mounted on insulating posts, oriented to measure the azimuthal field, and positioned $\sim 20 \text{ mm}$ from the liner with exact location recorded for each probe in every shot. The signal strength of each probe can be used to calculate a unique radius at which current must be flowing relative to the probe position, and correlation of this measurement for all probes defines the average position of the current density in the liner. This is completed for each set of 4 probes and the three axial positions. In this way, the evolution of the current density position on the azimuth of the liner can be determined. Imaging

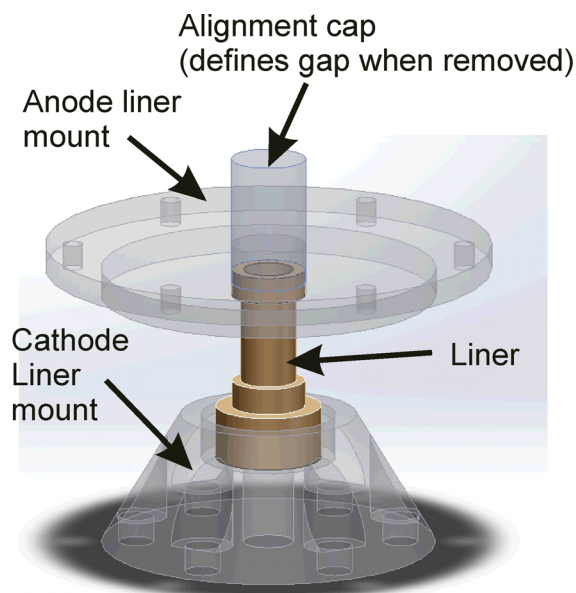


FIG. 1. Set-up for liner shots with an azimuthal gap at the anode.

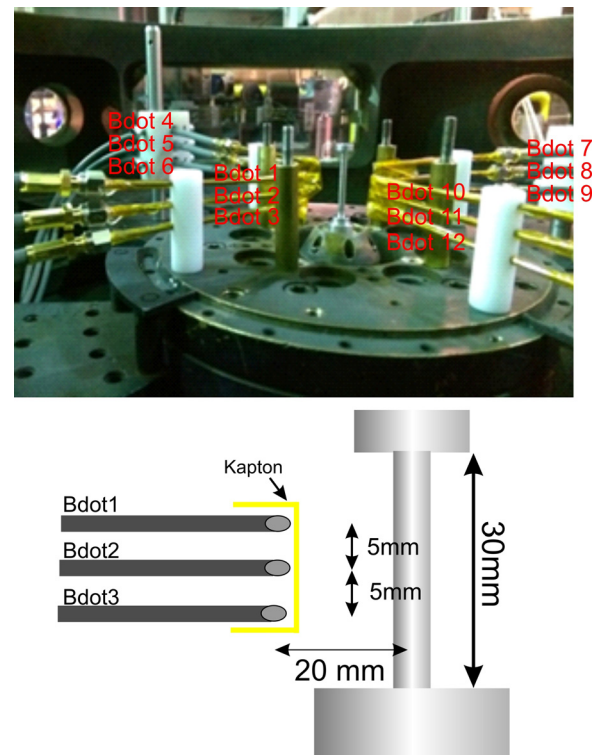


FIG. 2. Photograph and schematic of magnetic field probe array for 30 mm tall liners on COBRA. Probes 1, 2, and 3 are at 0° , probes 4, 5, and 6 at 90° , 7, 8, and 9 at 180° , and 10, 11, and 12 at 270° .

was also carried out using a multi-frame gated optical camera (Invisible Vision UHSi 12/24) imaging the load in the axial direction. This has a direct view of the vacuum power feed gap at the anode. Since up to 12 frames are possible in a single experiment, each with a 5 ns exposure time, these can be correlated with data from the bdot array.

RESULTS

Data were recorded from a number of shots on the COBRA generator, which typically delivered a current pulse of 1.0 MA in 120 ns to the aluminum liners discussed below. Timings are given relative to the start of the current pulse, defined as the departure of the measured dI/dt trace from the standard deviation of the pre-current noise level. Optical images show the formation of plasma at the anode gap which evolves on the timescale of the experiment. Typically, this begins as single or a small number of localized regions of emission, and these slowly expand as the drive current continues. Often new regions of emission are observed later in time, which also slowly expand. Even at late time, well after peak current, localization of the plasma in the gap dominates the emission profile in the majority of cases, and in no shot does the emission occupy the full azimuth of the liner for any shot performed using any gap size for this liner setup. An example of the optical imaging data is shown in Figure 3, which shows 8 frames taken during a single shot. Emission from plasma formed by the gap breakdown is typically observed at discrete locations $\sim 10\text{--}20 \text{ ns}$ into the current pulse, and are just visible in the 17 ns image in Fig. 3. In the 27 ns image, plasma is clearly visible, and there is a strong

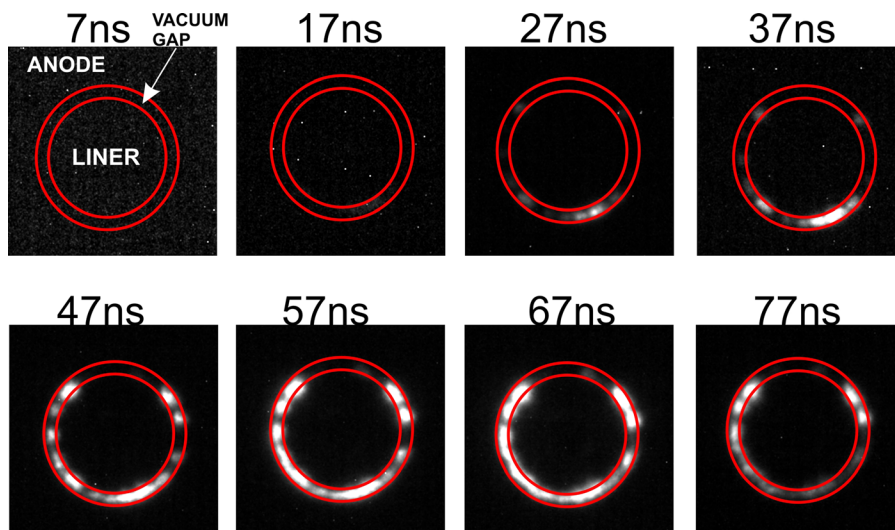


FIG. 3. Time sequence from the optical framing camera (5 ns exposure) showing evolution of the emission (plasma) profile for an aluminum liner with a $200\ \mu\text{m}$ anode power feed gap. Red circles bound the approximate location of the gap in the images.

variation in the intensity of each location emitting in the visible range observed by the camera. These regions are very similar and perhaps emitting more strongly in the 37 ns image. By 47 ns many of the same plasma regions are seen to be emitting again more strongly, but in addition, new regions have either developed or are now emitting strongly enough to be observed. This is a clear change from the previous image. As the current drive continues, the emission profile remains fairly static, with no new regions appearing and only some increase in intensity. Again note the large regions of the azimuth which show no emission throughout this experiment.

The image analysis relies on the gain and dynamic range of the camera, and indeed individual frames, so although the formation of plasma regions must be indicative of the current distribution, a more quantitative analysis is not possible. In Ref. 9, the liner shots primarily examined situations with a single primary breakdown, and in this case, a strong correlation of emission to the triangulated position of the current centroid is found. For situations where multiple emission regions appear and develop over time, interpretation is more complicated and indeed can be misleading in certain cases, as discussed below. Nevertheless, the limited extent of the azimuth which shows emission strongly suggests that the current generating and sustaining these plasmas is non-uniform in the liner itself.

The analysis of the magnetic field probe array data confirms this is almost always the case. An example is shown in Fig. 4, which shows an emission frame taken at 50 ns, and the triangulation plots for the three axial position examined by the bdot probe array. Note that the “top” position is closest to the imaging location which observes the anode. The circles on the photographs represent the signal strengths from each of the probes, centered on that probe. In an ideal case, overlap at a single position is observed, which reports the position of the centroid of the drive current on the liner load. As can be seen in Fig. 4, for the position at the top of the liner, the three probe signals overlap at the center of the liner, indicating that the current centroid is centered on the liner. Note that this does not necessarily denote uniform current flow in the liner as a whole, and indeed, the emission

image shows localized emission regions. Equally spaced plasma filaments carrying equal amount of the drive current will look identical to a uniform current on the triangulation plots. The use of both diagnostics in tandem can provide a useful physical interpretation in this case.

Since the magnitude of the B-field depends on $1/r$, as this increases the radius of the circle on the plots decrease, i.e., the current has moved closer to the probe. For the middle of the liner position in the same shot at the same time, the case is rather different than for the top. This is located only 5 mm below probes at the top on the liner, in the same azimuthal position on the same shot. The signal strength measured at probes 11 and 2 has increased (circles are smaller), indicating that the current centroid has moved to the bottom right of the liner. At the bottom of the liner, probe 9 shows the strongest signal (smallest circle), indicating the current is offset toward the top on the liner here. The location of the current in the liner differs with axial position at this time. Whilst the multiple regions of emission mean that an ideal triangulation overlap is not often observed, the relative strength of the probe signals gives a clear indication of the location of the average current for each location at any time in the shot.

The triangulation method plots in Figure 4 examine the axial variation in the current position for one time, but changes in the current position as the experiment proceeds can be clearly observed in the raw dB/dt traces recorded from the probes. If the current remains uniform throughout the current drive, the bdot probe signal should follow the current drive very closely. We can ensure this is the case by using a single wire in place of the liner, and mounting this offset to the center of the experiment. The current must remain in the wire throughout the drive current timescale. Results from such a shot are shown in Figure 5(a). This type of behavior is not observed for liner shots, where individual probes typically show significant deviation from the current form. Several examples are given in Figures 5(b)–5(d). In Figure 5(b), several bdot traces are shown to give a general overview of the data from a single shot. In Figure 5(c), we show a magnified region of Figure 5(b) (circle indicated). Until approximately 50 ns, the probes follow the form of the drive current. After this, the gradient of the probe 12 signal

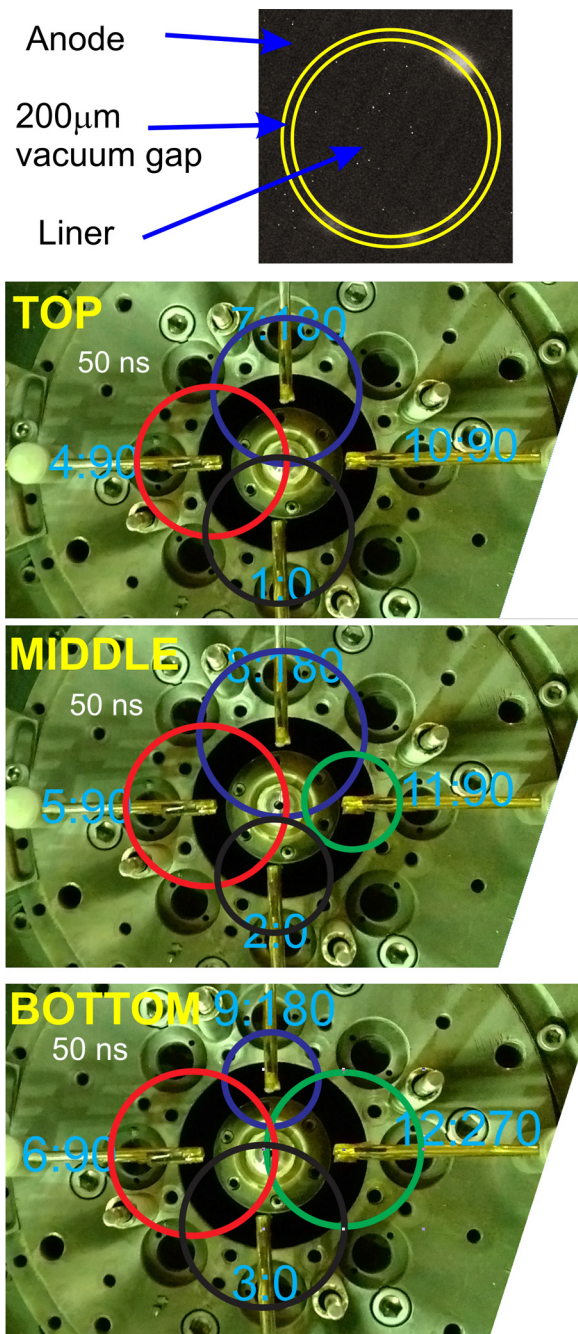


FIG. 4. Gated optical image at of aluminum liner experiment at 50 ns. Circles show triangulation of B-field signals for each probe position overlaid on photograph of liner experiment.

increases, and simultaneously, the gradient of probe 6 signal decreases. These probes are at the same axial position but on the opposite sides of the liner. This indicates that at 50 ns, the current centroid moves across the liner away from probe 6 and towards probe 12. At ~ 60 ns, probe 11 also shows a strong deviation from the current form, indicating that the current density is moving away from this probe position. Another example is shown in Fig. 5(d) from a different shot. Again probes 6 and 12 closely follow each other until 50 ns, after the signals strongly diverge, indicating motion of the current centroid towards probe 12 and away from probe 6. These data demonstrate that the current density shows

significant motion during the experiment, and such behavior is observed in every liner shot examined.

Given the formation of multiple regions of plasma which are all carrying some portion of the drive current, it is difficult to give quantitative values for the current density distribution from the bdot array triangulation methodology. However, the approximate portion of the azimuth in which the majority of the current flows can be inferred from the relative strengths of the bdot probe signals at any given time. This follows the methods described for the plots in Figure 4, and the full time evolution of the data for that shot is shown in Figure 6. The position of the majority of the current density is indicated by the red coloring at each axial position for each time in the sequence. Also shown are the optical imaging frames at the appropriate times. At 50 ns, the top triangulation shows a uniform current distribution, i.e., triangulation is centered on the liner as in Figure 4, whilst the middle is offset to the right and the bottom is offset to the rear right. At 60 ns, the top and middle are relatively unchanged, but the bottom is now primarily offset to the right. At 70 ns, the top no longer appears uniform, and is offset to the left, the middle remains offset to the right, and the bottom reverts to the rear right position seen earlier. After 70 ns, these positions remain relatively stable, at least as far as the triangulation method can detect. The differences observed between the three axial positions show that the current path is not necessarily directly in the axial direction during the experiment.

Figure 7 shows data from experiments where the vacuum gap was encouraged to breakdown in a predetermined location. This is achieved by placing a $100 \mu\text{m}$ wire into the vacuum gap mounted to the anode plate (a “trigger pin”). This effectively closes the gap to $100 \mu\text{m}$ in one azimuthal location, increasing the electric field, while the gap elsewhere remains at $200 \mu\text{m}$. The aim here is to determine if an initially non-uniform current distribution from a single breakdown position will rapidly become uniform throughout the liner. This would suggest that sufficient stand-off of the liner from a vacuum gap, i.e., physical distance along a transmission line, could be used to mitigate possible effects in other experiments. Results of two experiments using this arrangement are shown in Figure 7. In both cases, the position of the trigger pin causes breakdown at its location, and this has a significant effect on the emission and current density profile. In shot 3675, the only significant emission observed on the optical frames is at the location of the trigger pin throughout the experimental timescale, and emission at other azimuthal locations is not observed. The bdot array data give more detail on the evolution. The top level shows strong correlation of the current density to the location of the emission at the trigger pin through the experiment. The middle level is similar and centered on the trigger pin, although the triangulation is closer to the liner center, indicating a broader current density distribution. The bottom level starts initially centered on the liner but evolves to show a very similar distribution to the middle level as time proceeds.

For shot 3678, initially a similar process occurs. Initially, the only emission observed is close to the trigger pin, but at 80 ns, a large number of emission regions are observed opposite the trigger pin, and these persist through to the end of the experiment, gaining in intensity. This again is reflected in the

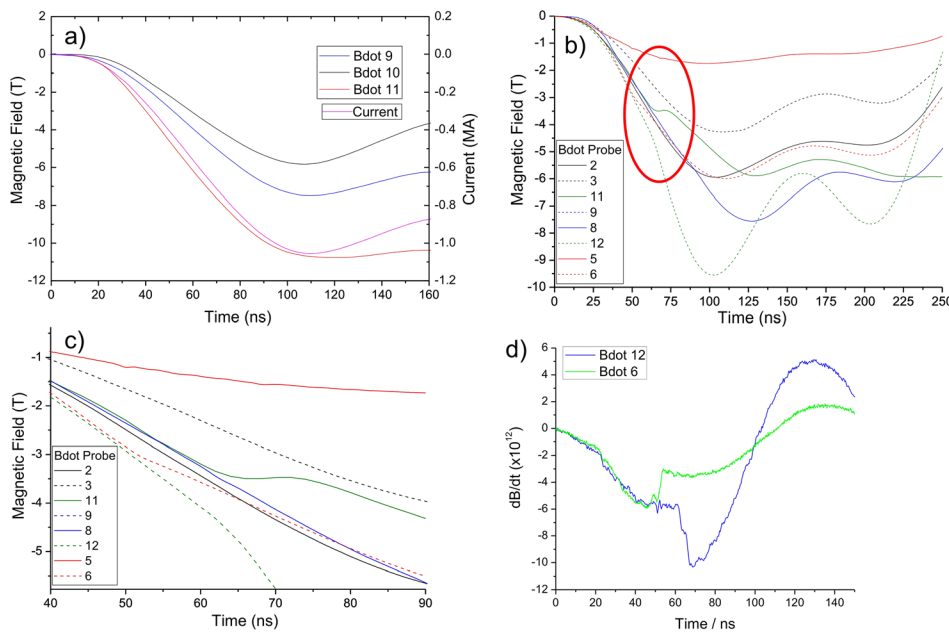


FIG. 5. Example magnetic field probe data showing deviation of measured B-field from current trend (e.g., see green trace bdot11 and text) indicating motion of the current density position in the liner.

bdot data. At 50 ns, all levels show current density closely aligned with the trigger pin position, with the top level significantly broader around the azimuth than the middle and bottom. The bottom remains fairly static through the experiment, but the middle and top show changes which appear correlated to the imaging data. At 70 ns, the middle level shows a far broader portion of the azimuth which is likely to be carrying current, i.e., the triangulation is nearly centered on the liner. This persists though to the 100 ns image. This change is reflected in the top level of probes in the 100 ns analysis. This suggests that the appearance of the additional emission regions late in time cause a redistribution of the current density around the liner, giving a more azimuthally uniform current, at least towards the top of the liner.

DISCUSSION

The experimental data show a rather complicated evolution of the current density. The simplest case is perhaps that of shot 3675 in Figure 7, where the liner shows offset current

density at the pin position which remains throughout the current drive. The drive voltage is applied to the load and forces electron emission at the pin position where the electric field is highest. The interaction of electrons and/or ions at the electrode surfaces deposit energy locally here and this generates a plasma which closes the gap, allowing current to flow in the load. At this point, the load voltage collapses and is then determined only by the current derivative $V=L \, dI/dt$ since the current rise rate is $\sim 10^{13} \text{ A/s}$ into an inductance of $\sim \text{few } 10\text{ s of nH}$. ($R = \text{few m}\Omega$ and dL/dt is zero as the load does not implode). The voltage is applied along the vertical axis, driving current in this direction, and once a conduction path is established, current flows here for the remainder of the experiment.

It should be noted that the bdot triangulation diagnostic cannot determine if current is flowing in a skin-depth in the liner or in surface plasma. For the COBRA current pulse, the collisionless skin depth is $\sim 50 \mu\text{m}$, and laser interferometry data does show the surface plasma formation at late time, although some of this is driven by the plasma formed at the

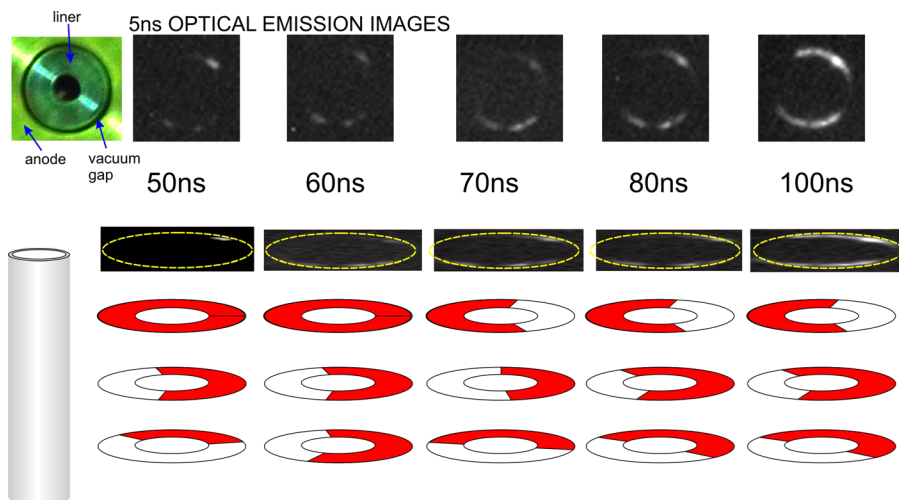


FIG. 6. Liner experiment data on COBRA showing optical emission frames along with the triangulation maps indicating the azimuthal position of the current density as a function of axial position and time.

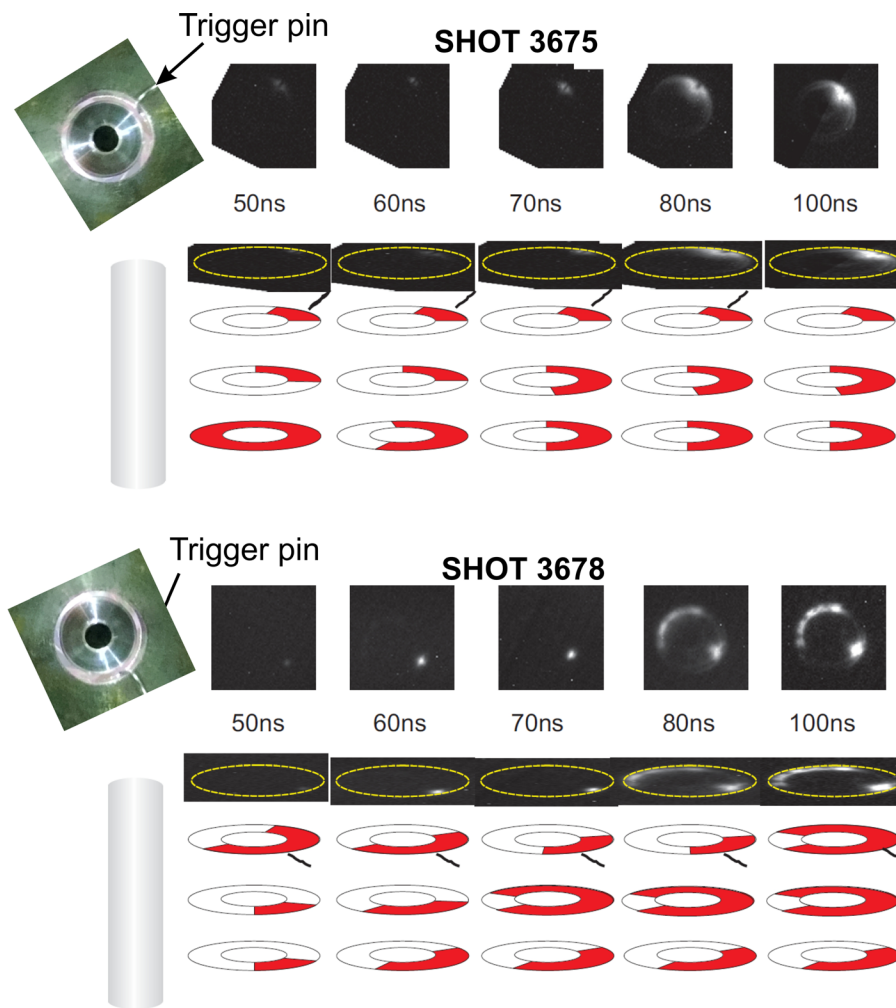


FIG. 7. Liner experiment data for loads using a trigger pin on COBRA, showing optical emission frames along with the triangulation maps indicating the azimuthal position of the current density as a function of axial position and time.

vacuum gap. The energy deposited in the liner in the initial resistive phase is typical low, \sim few joules, which for a solid liner results in only a small change in temperature. The formation of a surface plasma is unlikely in this case. However, once the main drive current begins to increase, the energy deposited through ohmic heating rapidly increases. The mass of aluminum in a skin depth for a 30 mm tall liner is $\sim 6.5 \times 10^{-5}$ kg, and the timescale for vaporization is ~ 5 ns, depending on the choice of resistivity.

The case where the current density remains static is limited to very few cases, and significant changes are observed with both pin triggered and non-triggered cases. In these, the evolution of the current density profile is slow. Magnetic field probe traces show significant gradient changes over timescales of ~ 5 – 10 ns, and this appears to correlate with changes in the axial emission profile observed via optical framing images. The current density profile must be driven by the divergence of the electric field (voltage) in a 3-dimensional object, along with the resistivity profile. Here, the use of a hollow liner, rather than a solid cylinder, means this appears as a 2-dimensional divergence, with the vector in the direction of the skin layer (towards the liner axis) eliminated since current cannot flow in the vacuum. The observed evolution timescale would appear more consistent with a diffusion process, as the current density is redistributed as a function of the liner and/or surface plasma resistivity evolution. This

may drive the formation of additional azimuthal breakdown positions at late time, which then carry some fraction of the current drive. However, it is not clear if this process would give rise to the non-axial current paths observed in experiments, and analytical calculations as a function of space and time at the liner surface are rather prohibitive.

To form additional breakdown position plasma streams at late time, a voltage is required at the position of the power feed gap. It is not clear, once breakdown across the vacuum gap has occurred, that there is a resistive voltage available to drive such a process, since current is already flowing. Indeed, as indicated above, the voltage at this time is purely inductive as indicated in experimental traces. One possibility is that multiple breakdown positions are formed at the initial application of the generator voltage, but that one path takes more current than the rest, perhaps due to more preferable resistivity conditions or easily ionized surface contaminants. If “secondary” paths at some azimuthal locations only take a small fraction of the current (e.g., 100s of amperes—check sensitivity), we would not observe this on the bdot triangulations, or on the optical imaging. If the ratio of the current in each stream remained fixed, for example, the diagnostic observation would only occur once they take enough current to be seen. This scenario obviates the need for a resistive voltage to drive later time streamer. It may be thought that inductance plays a role here too, since a uniform current

density around the liner is inductively more favorable, forcing all streamer to carry similar currents. However, in the COBRA experiments, the return posts are at large radii (>40 liner radii) so is likely to be a small factor in terms of the inductance reduction. This may play a role where a return structure is close to the liner, such as in the MagLIF experiments on the Z generator.

To summarize, whilst the evolution of the current density has been closely observed in these experiments, the mechanism driving the azimuthal current density distribution is yet to be determined. Magneto-hydrodynamic (MHD) simulations including accurate resistivity tables are currently underway and will address these issues directly.

CONCLUSIONS

Data show that non-uniformities in the initial current drive at one electrode persist throughout the entire drive time (100 ns) for 1 MA solid liners, and that current uniformity is not achieved using 30 mm tall liner targets. Additionally, the current density distribution is observed to change in almost all shots examined, and magnetic field probe data demonstrate clear examples of the current density moving around the liner azimuth during shots. The timescale of these motions is relatively slow and perhaps consistent with a resistive diffusion process or non-symmetric current distribution amongst several azimuthal locations. These hypotheses will be examined through 3D MHD simulations presently underway. Whilst data here are at the MA level, it suggests that in a reloading liner system for IFE, careful attention to the electrode-target interface is likely necessary to prevent a further source of non-uniformity in the compression phase. A good example is a knife-edge type method as discussed in Ref. 8. Loading schemes which use a “push-fit” still leave vacuum gaps which can drive asymmetry in the azimuthal current distribution and should be avoided.

ACKNOWLEDGMENTS

This work was supported under National Nuclear Security Administration Stockpile Stewardship Academic

Alliance (NNSA SSAA) program through DOE Cooperative Agreement No. DE-NA0001836. The authors also wish to thank Todd Blanchard and Harry Wilhelm for supporting the experimental campaigns on COBRA.

- ¹R. E. Reinovsky, W. E. Anderson, W. L. Atchison, C. E. Ekdahl, R. J. Faehl, I. R. Lindemuth, D. V. Morgan, M. Murillo, J. L. Stokes, and J. S. Shlachter, *IEEE Trans. Plasma Sci.* **30**, 1764 (2002).
- ²D. B. Sinars, S. A. Slutz, M. C. Herrmann, R. D. McBride, M. E. Cuneo, K. J. Peterson, R. A. Vesey, C. Nakhleh, B. E. Blue, K. Killebrew, D. Schroen, K. Tomlinson, A. D. Edens, M. R. Lopez, I. C. Smith, J. Shores, V. Bigman, G. R. Bennett, B. W. Atherton, M. Savage, W. A. Stygar, G. T. Leifeste, and J. L. Porter, *Phys. Rev. Lett.* **105**, 185001 (2010).
- ³J. H. Degnan, J. M. Taccetti, T. Cavazos, D. Clark, S. K. Coffey, R. J. Faehl, M. H. Frese, D. Fulton, J. C. Gueits, D. Gale *et al.*, *IEEE Trans. Plasma Sci.* **29**, 93 (2001).
- ⁴R. D. McBride, M. R. Martin, R. W. Lemke, J. B. Greenly, C. A. Jennings, D. C. Rovang, D. B. Sinars, M. E. Cuneo, M. C. Herrmann, S. A. Slutz, C. W. Nakhleh, D. D. Ryutov, J.-P. Davis, D. G. Flicker, B. E. Blue, K. Tomlinson, D. Schroen, R. M. Stamm, G. E. Smith, J. K. Moore, T. J. Rogers, G. K. Robertson, R. J. Kamm, I. C. Smith, M. Savage, W. A. Stygar, G. A. Rochau, M. Jones, M. R. Lopez, J. L. Porter, and M. K. Matzen, *Phys. Plasmas* **20**, 056309 (2013).
- ⁵S. A. Slutz, M. C. Herrmann, R. A. Vesey, A. B. Sefkow, D. B. Sinars, D. C. Rovang, K. J. Peterson, and M. E. Cuneo, *Phys. Plasmas* **17**, 056303 (2010).
- ⁶C. L. Olsen, *Inertial Confinement Fusion: Z-pinch*, Volume 3B of the series Landolt-Börnstein - Group VIII Advanced Materials and Technologies, Chap. 9, pp. 495–528.
- ⁷I. C. Blesener, K. S. Blesener, J. B. Greenly, D. A. Hammer, B. R. Kusse, C. E. Seyler, and B. Blue, “Ablation dynamics, precursor formation, and instability studies on thin foil copper liners,” in *Proceedings of IEEE International Conference on Plasma Science, Chicago, IL, Jun. 26–30, 2011*, p. 1.
- ⁸T. J. Awe, B. S. Bauer, S. Fuelling, and R. E. Siemon, *Phys. Rev. Lett.* **104**, 035001 (2010).
- ⁹S. W. Cordaro, S. C. Bott-Suzuki, L. S. Caballero Bendixsen, L. Atoyan, T. Byvank, W. Potter, B. R. Kusse, and J. B. Greenly, *Rev. Sci. Instrum.* **86**, 073503 (2015).
- ¹⁰S. C. Bott-Suzuki, S. W. Cordaro, L. S. Caballero Bendixsen, I. C. Blesener, L. Atoyan, T. Byvank, W. Potter, K. S. Bell, B. R. Kusse, and J. B. Greenly, *Phys. Plasmas* **22**, 094501 (2015).
- ¹¹J. B. Greenly, J. D. Douglas, D. A. Hammer, B. R. Kusse, S. C. Glidden, and H. D. Sanders, *Rev. Sci. Instrum.* **79**, 073501 (2008).
- ¹²J. Greenly, M. Martin, I. Blesener, D. Chalenski, P. Knapp, and R. McBride, *AIP Conf. Proc.* **1088**, 53 (2009).